

# Modeling of holographic gratings in photorefractive graded-index planar waveguides

Vittorio M. N. Passaro, Daniele Marseglia  
Optoelectronics Laboratory, Dipartimento di Elettrotecnica ed Elettronica  
Politecnico di Bari, Via Edoardo Orabona 4 – 70125 Bari, Italy  
[passaro@poliba.it](mailto:passaro@poliba.it), [maddanny@libero.it](mailto:maddanny@libero.it)

In this paper an accurate modeling of both collinear and non collinear wave interaction in the formation of holographic gratings in photorefractive graded-index planar waveguides is presented. Results for lithium niobate waveguide technologies are given.

**Keywords:** holographic gratings, lithium niobate waveguides, photorefractive effect, modeling.

## Introduction

Nowadays, a significant research interest is devoted to the holographic grating formation in photorefractive waveguides, whose deep knowledge should lead to design new types of integrated optical devices. In fact, light beams in optical planar waveguides are confined in one dimension to regions only a few micrometers in width and so the high optical intensities, which are thus readily obtained, make it relatively easy to observe effects of photorefractivity to be used in integrated photorefractivity-based devices [1]. In recent literature it is possible to find a lot of examples, such as linear filters providing for high-resolution spectral filtering [2], beam splitters and couplers [3] or dynamic interconnections for neural networks [4]. With the aim to design such devices with high accuracy, we have developed a numerical model of the holographic grating formation in graded-index planar waveguides, which is not yet available in literature.

## Theoretical model

The model can analyze the holographic grating formation in arbitrary graded-index waveguides having a generic electro-optic crystal ( $r_{ij}$  tensor), both in case of collinear and non collinear, intermode and intramode wave interaction. This paper is based on the extension of the model presented in [5]. Fig. 1 shows the vector diagram of the non collinear interaction geometry, where  $\rho$  is the propagation direction,  $\tau$  is the transverse direction,  $\vec{K}_A$  and  $\vec{K}_B$  are the incidence vectors of the interacting fields  $A$  and  $B$ , respectively,  $\vec{K}_g$  is the induced grating vector and  $\mathcal{G}_c$  is the crossing angle. Furthermore, an arbitrary overlay can be also taken into account.

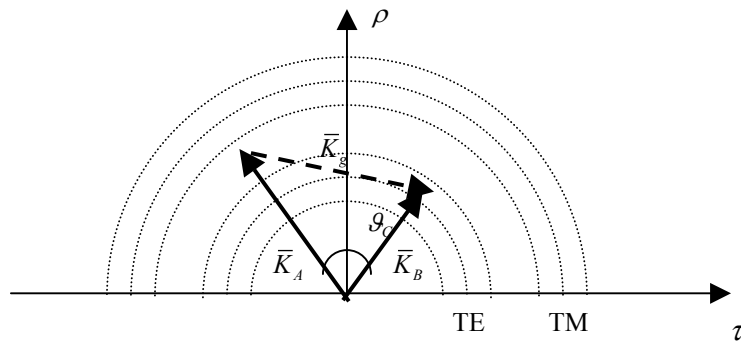


Fig. 1. Vector diagram for a non collinear interaction between two generic modes,  $A$  and  $B$ .

It is well known that the perturbations of the dielectric permittivity tensor  $\varepsilon_{ij}$ , caused by the photorefractive effect, are physically related to the photo-induced potential distribution,  $\varphi$ .

For a generic mode interaction (i.e. either intermode or intramode), we have derived from the continuity equation (see [6]) the equation of induced oscillations, considering only the photogalvanic current (neglecting the diffusion current) and admitting that the its spatially oscillating components depend only on the cut-axis (hereinafter named *cut*). In the absence of any applied electric field and assuming the cut-axis and the direction of propagation both coincident with the crystallographic axes, the equation of induced oscillations can be written in the very general formulation as follows:

$$\frac{d^2\varphi}{dcut^2} - K_g^2 \frac{\varepsilon_\rho^S}{\varepsilon_{cut}^S} \varphi = f(t) \frac{t_0}{\varepsilon_{cut}^S} \left( -jK_g \delta_\rho^{ph} + \frac{\partial \delta_{cut}^{ph}}{\partial cut} \right) \quad (1)$$

where  $K_g$  is the grating vector amplitude [7], i.e.  $K_g = |\bar{K}_g|$ ,  $\varepsilon_{cut}^S$  and  $\varepsilon_\rho^S$  are the static (i.e. without any interaction) dielectric tensor components along the *cut*-axis and  $\rho$ -axis, respectively, and  $\delta_{cut}^{ph}$  and  $\delta_\rho^{ph}$  are the photogalvanic current components along the *cut*-axis and  $\rho$ -axis, respectively. The physical meaning of the characteristic time  $t_0$  and function  $f(t)$  can be better understood by discussing about  $\varphi$ . In fact, the photo-induced potential  $\varphi$  can be explicated as follows:

$$\varphi = \varphi(cut, \rho, t) = \varphi_0(cut, t_0) f(t) \exp(-j \langle \bar{K}_g \rangle_\rho) \quad (2)$$

where the function  $\varphi_0 = \varphi_0(cut, t)$  represents the photo-induced potential for the initial recording section, when the conductivity currents are negligible, and its dependence on time and spatial coordinates have been simultaneously considered.  $\langle \bar{K}_g \rangle_\rho$  is the  $\bar{K}_g$  projection along  $\rho$ -axis.

Furthermore, by neglecting the photo-conductivity respect to the dark conductivity  $\sigma^d$ ,  $f(t)$  is an increasing exponential function (having the Maxwell relaxation time  $\tau_m$  as a time constant) and  $t_0$  is equal to  $\tau_m$  [6]. We remember that  $\tau_m = \varepsilon_{cut}^S / \sigma_{cut}^d$ , where  $\sigma_{cut}^d$  is the dark conductivity component along *cut*-axis.

The photogalvanic current is strictly related to the photogalvanic tensor  $\beta$ , which depends on the structure considered. For a graded-index waveguide  $\beta$  changes along the *cut* axis,  $\beta = \beta(cut)$ . However, it is possible to define an effective photogalvanic tensor  $\tilde{\beta}$ , which can be evaluated by a quasi-empirical model [6]. We can evaluate the photogalvanic current vector as follows:

$$\delta^{ph} = \beta E^A E^{B*} \exp(-j \langle \bar{K}_g \rangle_\rho) \quad (3)$$

where  $E^A$  and  $E^B$  are the electric field vectors of two generic guided modes  $A$  and  $B$ , respectively. In this way, our model is applicable to both an intermode and intramode interaction, without any restriction over the incidence angle. Therefore, by using Eqns. (1), (2) and (3), we can write the equation of induced oscillations as

$$\frac{d^2\varphi_0}{dcut^2} - K_g^2 \frac{\varepsilon_\rho^S}{\varepsilon_{cut}^S} \varphi_0 = \frac{t_0}{\varepsilon_{cut}^S} \left( -jK_g \langle \beta E^A E^B \rangle_\rho + \frac{\partial}{\partial cut} \langle \beta E^A E^B \rangle_{cut} \right) \quad (4)$$

The numerical solution of Eqn. (4) allows to evaluate the perturbations of the dielectric tensor components  $\Delta\varepsilon_{ij}$  (as a multidimensional array), or otherwise, of the permeability tensor

components by the linear electro-optic effect, as in [5], by which each information about the holographic grating properties can be derived.

## Numerical results

In the numerical results, we have assumed z-propagation for X-cut, and x-propagation for Y-cut and Z-cut. As a first example, we have considered a Ti:LiNbO<sub>3</sub> Gaussian index profile waveguide ( $\Delta n_{e\max} \cong 0.0005$ ,  $\Delta n_{o\max} \cong 0.001$ ), at room temperature ( $T = 300$  K), wavelength  $\lambda = 632.8$  nm, without any overlay. In Fig. 2, the largest value of dielectric tensor perturbation is shown as a function of the crossing angle  $\theta_C$ . The other components are found to be at least one order of magnitude lower with respect to the largest one. Of course, the photorefractive sensitivity is strongly related to this main component. From Fig. 2 we can see the comparison among various substrate cuts and non collinear mode interactions, i.e. TE<sub>0</sub>-TM<sub>0</sub> in Y-cut ( $\Delta\varepsilon_{23}$ ), TM<sub>0</sub>-TM<sub>0</sub> in Y-cut ( $\Delta\varepsilon_{23}$ ), TE<sub>0</sub>-TM<sub>0</sub> in Z-cut ( $\Delta\varepsilon_{33}$ ) and TE<sub>0</sub>-TE<sub>0</sub> in Z-cut ( $\Delta\varepsilon_{33}$ ).

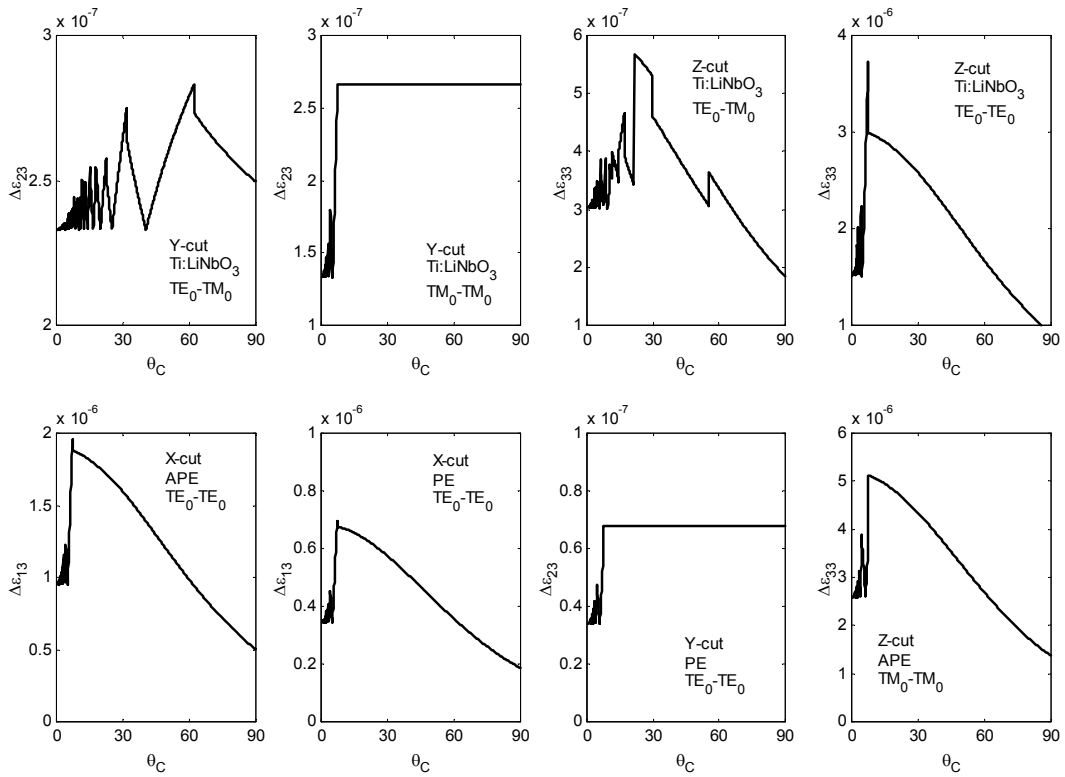


Fig. 2. Dielectric tensor main perturbation dependence on the crossing angle.

Similarly, at constant wavelength and temperature, we have considered a proton exchanged (PE) waveguide (step-index profile,  $\Delta n_o = 0$  and  $\Delta n_e = 0.01$ , and strongly reduced electro-optic activity,  $r \cong r/10$  in the highly protonated layer) and an annealed PE (APE) waveguide (exponential profile;  $\Delta n_{o\max} = 0.005$  and  $\Delta n_{e\max} = 0$ , and partially restored electro-optic activity,  $r \cong r/2$ ). In Fig. 2, the largest dielectric perturbations are sketched for the TE<sub>0</sub>-TE<sub>0</sub> interaction in a X-cut LiNbO<sub>3</sub> waveguide, by assuming either an APE ( $\Delta\varepsilon_{13}$ ) or a PE technology ( $\Delta\varepsilon_{13}$ ), the TE<sub>0</sub>-TE<sub>0</sub> interaction in an Y-cut PE:LiNbO<sub>3</sub> waveguide ( $\Delta\varepsilon_{23}$ ), and TM<sub>0</sub>-TM<sub>0</sub> interaction in an Z-cut APE:LiNbO<sub>3</sub> waveguide ( $\Delta\varepsilon_{33}$ ). We can see from Fig. 2 that a similar angle can be recognized for all the

intramode interactions where the perturbation is maximum, about  $7.5^\circ$ , the value remaining constant only for Y-cut substrate. Moreover, we have carried out a number of simulations changing the fabrication technology and crystal cut, in case of collinear geometry. We have evaluated and compared the order of magnitude of all the induced dielectric tensor perturbations. Table I summarizes the results in a normalised form, where the components lower than  $10^{-8}$  have been considered negligible ( $\sim 0$ ).

Table I. Comparison among different LiNbO<sub>3</sub> technologies (T = 300 K,  $\lambda = 632.8$  nm).

Cut	Technology	Interaction	$\Delta\varepsilon_{11}$	$\Delta\varepsilon_{12}$	$\Delta\varepsilon_{13}$	$\Delta\varepsilon_{22}$	$\Delta\varepsilon_{23}$	$\Delta\varepsilon_{33}$
X	Ti-diffused	TE <sub>0</sub> -TM <sub>0</sub>	$\sim 0$	10	100	$\sim 0$	$\sim 0$	$\sim 0$
		TE <sub>0</sub> -TE <sub>0</sub>	$\sim 0$	10	100	$\sim 0$	$\sim 0$	$\sim 0$
		TM <sub>0</sub> -TM <sub>0</sub>	$\sim 0$	10	100	$\sim 0$	$\sim 0$	$\sim 0$
	APE	TE <sub>0</sub> -TE <sub>0</sub>	$\sim 0$	10	100	$\sim 0$	$\sim 0$	$\sim 0$
	PE	TE <sub>0</sub> -TE <sub>0</sub>	$\sim 0$	1	10	$\sim 0$	$\sim 0$	$\sim 0$
Y	Ti-diffused	TE <sub>0</sub> -TM <sub>0</sub>	1	$\sim 0$	$\sim 0$	1	10	$\sim 0$
		TE <sub>0</sub> -TE <sub>0</sub>	1	$\sim 0$	$\sim 0$	1	10	$\sim 0$
		TM <sub>0</sub> -TM <sub>0</sub>	1	$\sim 0$	$\sim 0$	1	10	$\sim 0$
	APE	TE <sub>0</sub> -TE <sub>0</sub>	1	$\sim 0$	$\sim 0$	1	10	$\sim 0$
	PE	TE <sub>0</sub> -TE <sub>0</sub>	$\sim 0$	$\sim 0$	$\sim 0$	$\sim 0$	1	$\sim 0$
Z	Ti-diffused	TE <sub>0</sub> -TM <sub>0</sub>	1	$\sim 0$	$\sim 0$	1	$\sim 0$	10
		TE <sub>0</sub> -TE <sub>0</sub>	10	$\sim 0$	1	10	$\sim 0$	100
		TM <sub>0</sub> -TM <sub>0</sub>	10	$\sim 0$	1	10	$\sim 0$	100
	APE	TM <sub>0</sub> -TM <sub>0</sub>	10	$\sim 0$	1	10	$\sim 0$	100
	PE	TM <sub>0</sub> -TM <sub>0</sub>	1	$\sim 0$	$\sim 0$	1	$\sim 0$	10

From Table I, the best technological conditions for high efficiency guided-wave holographic devices can be easily found. Other calculations obtained by including an overlay (refractive index 1.5, 2  $\mu\text{m}$  in depth) have shown similar results.

## Conclusions

The numerical analysis of the dielectric tensor perturbations by photorefractive effect in graded-index planar waveguides has been presented. A powerful software tool has been developed to investigate any kind of guided mode interaction, i.e. collinear or not-collinear and either intermode or intramode interaction. Related results have been presented to select the best condition, i.e. the crossing angle, the crystal cut and the waveguide fabrication technology, in terms of the maximum sensitivity, to be used for design purposes.

- [1] V. E. Wood, P. J. Cressman, R. L. Holman and C. M. Verber, *Photorefractive Materials and their Applications II* **62**, 45-100, Springer-Verlag, Berlin, 1988.
- [2] T. W. Mossberg, *Optics Letters* **26**, 414-416, 2001.
- [3] K. Itoh, K. Ikewaza, W. Watanabe, Y. Furuya and Y. Masuda, *Opt. Express* **2**, 503-508, 1998.
- [4] O. Matoba, K. Ikewaza, K. Itoh and Y. Ichioka, *Opt. Review* **2**, 438-443, 1995.
- [5] V. M. N. Passaro and D. Marseglia, *Opt. Express* **10**, 1133-1138, 2002.
- [6] G. Glazov et al., *J. Opt. Soc. Am. B* **7**, 2279-2288, 1990.